ELSEVIER

Journal of Environmental Management 84 (2007) 336–346

Journal of Environmental Management

www.elsevier.com/locate/jenvman

Modeling manure-borne bromide and fecal coliform transport with runoff and infiltration at a hillslope

M.Y. Kouznetsov[a], R. Roodsari[b], Y.A. Pachepsky[c,*], D.R. Shelton[c], A.M. Sadeghi[d], A. Shirmohammadi[b], J.L. Starr[d]

[a]*Jacob Blaustein Institute for Desert Research, Ben Gurion University of the Negev, Israel*
[b]*Department of Biological Resources Engineering, University of Maryland, College Park, USA*
[c]*USDA-ARS Environmental Microbial Safety Laboratory, Beltsville, MD, USA*
[d]*USDA-ARS Environmental Quality Laboratory, Beltsville, MD, USA*

Received 16 July 2005; received in revised form 5 June 2006; accepted 6 June 2006
Available online 28 August 2006

Abstract

Hillslope vegetated buffers are recommended to prevent water pollution from agricultural runoff. However, models to predict the efficacy of different grass buffer designs are lacking. The objective of this work was to develop and test a mechanistic model of coupled surface and subsurface flow and transport of bacteria and a conservative tracer on hillslopes. The testing should indicate what level of complexity and observation density might be needed to capture essential processes in the model. We combined the three-dimensional FEMWATER model of saturated–unsaturated subsurface flow with the Saint-Venant model for runoff. The model was tested with data on rainfall-induced fecal coliforms (FC) and bromide (Br) transport from manure applied at vegetated and bare 6-m long plots. The calibration of water retention parameters was unnecessary, and the same manure release parameters could be used both for simulations of Br and FC. Surface straining rates were similar for Br and bacteria. Simulations of Br and FC concentrations were least successful for the funnels closest to the source. This could be related to the finger-like flow of the manure from the strip along the bare slopes, to the transport of Br and FC with manure colloids that became strained at the grass slope, and to the presence of micro-ponds at the grassed slope. The two-dimensional model abstraction of the actual 3D transport worked well for flux-averaged concentrations. The model developed in this work is suitable to simulate surface and subsurface transport of agricultural contaminants on hillslopes and to evaluate efficiency of grass strip buffers, especially when lateral subsurface flow is important.
Published by Elsevier Ltd.

Keywords: Overland flow; Infiltration; Fecal coliforms; Manure; Modeling

1. Introduction

Large quantities of manure are routinely applied on soil in crop production and in grazing land systems as a source of nutrients for plant growth. However, manures also contain large numbers of microorganisms, some of which may be pathogenic to humans. Nutrients and microorganisms are released in runoff as manures dissolve during rainfall events. Vegetated filter strips (VFS) have become a widespread management practice for reducing the level of nutrients and microorganisms in runoff, thereby minimizing the contamination of surface waters (Sanderson et al., 2001; Abu-Zreig et al., 2003).

The mechanisms of the VFS functioning related to surface water quality include (a) reducing flow capacity, resulting in loss of transport capacity which leads to deposition of sediment and adsorbed potential pollutants, (b) enhancing infiltration of water and chemicals into soil matrix, and (c) adsorbing chemicals onto the litter, vegetation, and surface layer of soil, all of which reduce the outflow concentration (Johnson and Moore, 1978;

Abbreviations: FC, Fecal coliform(s); CV, Coefficient of variation; VFS, Vegetated filter strips

*Corresponding author. Tel.: +1 301 504 7468; fax: +1 301 504 6608.
E-mail address: ypachepsky@anri.barc.usda.gov (Y.A. Pachepsky).

0301-4797/$ - see front matter Published by Elsevier Ltd.
doi:10.1016/j.jenvman.2006.06.011

Crane et al., 1983). There is no consensus in the literature on whether these mechanisms have similar quantitative effects on nutrient and microbial transport. Several studies (McCaskey et al., 1971; Crane et al., 1983; Bartfield et al., 1998) suggest that the VFS removal of chemical constituents from runoff is unrelated to bacteria removal, indicating that the transport mechanisms may be different for bacterial and chemical manure constituents. Other authors (Edwards et al., 1996a, b; Roodsari, et al., 2005) indicate that all manure-borne constituents are transported primarily in solution phase and that their transport is not substantially affected by deposition of particulate components. In this case, the VFS design should be based solely on partitioning between runoff and infiltration regardless of the type of constituent.

The difficulty in predicting the relative transport rates of manure-borne microorganisms vs. solutes is due, in large measure, to the lack of appropriate models. Considering that infiltration is an important factor in the VFS functioning, appropriate models need to account for both surface and subsurface and flow conditions. A vertical cross-section of a hillslope gives a two dimensional representation of the conditions for surface and subsurface flow and transport. Such representation is important when the subsurface flow is essentially two dimensional because of soil and sediment layering, presence sediment lenses, shape of the ground water surface causing seepage at the slope, presence of perched horizons, and substantial lateral flow that may be preferential.

The objective of this study was to use a coupled two-dimensional surface–subsurface flow and transport model to test the hypothesis that the parameters of transport in surface runoff are close for manure-borne fecal coliforms (FC) and bromide-ion. To our knowledge, a model for this purpose has not been previously proposed.

2. Materials and methods

2.1. Modeling two-dimensional coupled surface–subsurface water flow and solute transport at a hillslope

2.1.1. Equations of the model

The overland flow was simulated using the Saint-Venant equations:

$$\frac{\partial h}{\partial t} = -\frac{\partial q}{\partial l} + R - I \tag{1}$$

and

$$\frac{\partial q}{\partial t} = -\frac{\partial}{\partial l}\left(\frac{q^2}{h} + \frac{gh^2}{2}\right) + gh(S_0 - S_f), \tag{2}$$

here h is the flow depth, m; q the discharge per unit width, $m^2\,s^{-1}$; g the acceleration due to gravity, ms^{-2}; R the rainfall rate, $m\,s^{-1}$; I the infiltration rate, $m\,s^{-1}$; S_0 the bottom slope in the direction of flow; S_f the friction slope; l the distance along the flow direction, m, and t is the time, s. The friction slope was computed using the Manning formula:

$$S_f = \frac{(nq)^2}{h^{10/3}}, \tag{3}$$

where n is the Manning roughness coefficient, $m^{-1/3}\,s$. The surface flow boundary condition is the zero flux at the top of the slope and the initial conditions are

$$h(l,0) = 0; \quad q(l,0) = 0. \tag{4}$$

The two-dimensional Richards equation is used to simulate water flow in soil as described in Richards et al. (1997). The subsurface flow domain is the quadrilateral with the upper side on the soil surface, the bottom side parallel to the upper side at the 60-cm depth, and two vertical sides at the top and the bottom of the slope. The unsaturated soil hydraulic properties were expressed using the van Genuchten–Mualem equations (Van Genuhten, 1980):

$$S = \frac{1}{[1 + (\alpha h)^n]^m}, \tag{5}$$

$$K = K_{sat}(S)^l[1 - (1 - S^{1/m})^m]^2. \tag{6}$$

In Eqs. (5) and (6), S is the soil saturation, $S = (\theta - \theta_r)/(\theta_s - \theta_r)$, θ the volumetric water content, h the capillary pressure (the absolute value of the matrix potential), ϕ the porosity, θ_s the saturated water content, θ_r the residual water content, K_{sat} the saturated hydraulic conductivity, and α, m, n, and l are empirical shape-defining parameters.

The boundary conditions are (a) zero flux at the vertical sides, (b) free seepage at the bottom, and (c) the infiltration flux is equal to rainfall intensity in the absence of runoff and soil water potential is equal to h in the presence of runoff at the soil surface. The initial soil water potential ψ_0 is set constant across the flow domain.

The overland transport of solutes is simulated as an advective–dispersive process with possible reversible concentration-dependent attachment–detachment, possible irreversible straining, nonlinear dissolution kinetics, and advective–dispersive mass exchange with subsurface:

$$\frac{\partial(ch)}{\partial t} + \frac{\partial c_s}{\partial t} = -\frac{\partial(cq)}{\partial l} + \frac{\partial}{\partial l} D_d \frac{\partial c}{\partial l} - \lambda hc + Q, \tag{7}$$

here $c(l,t)$ is the solute concentration in the runoff, $M\,m^{-3}$, where M is defined as the number of colony forming units (CFU) for bacteria $\times 10^6$, and as g for the Br^-, c_s is the surface density of the adsorbed solute, $M\,m^{-2}$, $c_s = K_F c^{n_F}$, K_F and n_F parameters of the Freundlich equation for the mass-exchange isotherm, $D_d = hD_m + \alpha q$ is the dispersion coefficient, $m^3\,s^{-1}$, D_m is the molecular diffusion coefficient, α is the longitudinal dispersivity, m, λ is the straining rate coefficient, s^{-1}, Q is the solute mass influx to runoff, $M\,m^{-2}\,s^{-1}$. The value of Q consists of two components Q_1 and Q_2 ($Q = Q_1 + Q_2$). Here Q_1 is the rate of the solute

mass influx from dissolving sludge,

$$Q_1 = K_r\left(\frac{m}{m_0}\right)^p, \tag{8}$$

where m is the mass of the solute in the manure sludge on soil surface, $\mathrm{M\,m^{-2}}$, m_0 the initial value of m, K_r the release rate constant, $\mathrm{M\,m^{-2}\,s^{-1}}$, and p the empirical exponent. The second component, Q_2 the rate of the solute loss from runoff to soil with infiltration, $\mathrm{M\,m^{-2}\,s^{-1}}$, $Q_2 = cI$. The solute mass conservation in the sludge is simulated with

$$\frac{\partial m}{\partial t} = -Q_1. \tag{9}$$

The subsurface solute transport is simulated with the two-dimensional advective–dispersive equation with possible reversible attachment–detachment according the linear isotherm of attachment, and possible first-order kinetic straining as described by Richards et al. (1997). Boundary conditions are (a) zero flux at vertical sides, (b) zero gradient at the bottom, and (c) zero flux in absence of runoff and the concentration in soil water equal to the concentration in runoff in the presence of runoff at the soil surface. Initial solute concentration in subsoil is set to zero.

2.1.2. Numerical solution

The system of the surface flow Eqs. (1), (2) was solved using the non-oscillatory algorithm of Sanders and Iahr (2001). The solute transport equation was solved using the implicit–explicit finite difference method with the front limitation algorithm (Haefner et al., 1997). The FEMWATER code was used to solve the subsurface flow and transport problems. The flow problem in this code was solved using the explicit finite element method, and the transport problem was solved with the Lagrangian–Eulerian finite element method (Richards et al., 1997).

The surface and subsurface flow and transport algorithms alternated as suggested by Singh and Bhallamudi (1998): (1) the subsurface flow solution at time level n was used to determine the infiltration rate at the soil surface, (2) surface flow equations were solved using the infiltration rate from the step 1 to determine q and h at the unknown time level $n+1$, (3) surface transport equations were solved with those values of q and h, (4) the surface flow depth at the time level $n+1$ was used as the top boundary condition and the subsurface flow equations were solved, thus giving distributions of soil water contents and soil water potentials, (4) the subsurface transport equations were solved. The Courant criterion

$$C_n = \frac{\Delta t}{\Delta x}\left(\frac{q}{h} + \sqrt{gh}\right) \leqslant 1.0 \tag{10}$$

was used to select time step.

Two small parameters were introduced to prevent oscillations and to save computing time. First, as it was suggested by Singh and Bhallamudi (1998), runoff was deemed to be formed and solution of the Eqs. (1) and (2) began when the soil matric potential on the surface exceeded a small positive number h_0 that can be viewed as an initial thickness of the water film on the surface. This value was used as an initial condition for Eq. (1). A corresponding value of the discharge q_0 is computed according to Eq. (4) with $h = h_0$ and is used as the initial condition for the Eq. (2). Second, as suggested by Kouznetsov (1989) the boundary conditions of the subsurface flow at soil surface were written in a unified form as

$$\frac{\partial(\eta(h)h)}{\partial t} = R - I, \tag{11}$$

where the Heavyside function is

$$\eta(h) = \begin{cases} 1, & h \geqslant 0, \\ 0, & h < 0, \end{cases} \tag{12}$$

and the discontinuous Heavyside function and its derivative the Dirak function are replaced with their continuous approximations

$$\eta_\omega(h) = \frac{1}{\pi}\,\mathrm{arctg}(h/\omega)h,$$
$$\delta_\omega(h) = \frac{1}{\pi}\frac{\omega}{\omega^2 + h^2}, \tag{13}$$

where ω is a calibration parameter. This allowed avoiding iterations to find the ponding time in each of surface nodes. The unified boundary condition (11) was applied while the soil matric potential on surface was less than h_0.

Ponding did not generally occur simultaneously in all surface nodes, and the ponding front moved along the slope until all nodes were ponded. The progress of the ponding front was simulated by adding the runoff discharge from the latest ponded node to the rainfall in the node where ponding was expected to occur and where the unified boundary condition was applied. This procedure required small time steps of about 1 s to achieve the satisfactory accuracy. The time step values were found from the sensitivity analysis to achieve the 1% difference in runoff values simulated with selected and halved time steps.

The model and computer code were tested with the experimental data of Smith and Woolhiser (1971). Their experiments were conducted with a 12.2 m long and 1.22 m deep soil flume. The fluid was light oil with a kinematic viscosity of $1.94 \times 10^{-6}\,\mathrm{m^2\,s^{-1}}$. The rainfall simulator generated rainfall of intensity $0.25\,\mathrm{m\,h^{-1}}$ for 15 min. The flume was filled with three layers of sand with different hydraulic properties. The data on hydraulic properties of the layers were approximated by Singh and Bhallamudi (1998) with

$$k = K_s F(\psi, a_{1k}, a_{2k}, a_{3k}, \psi_{1k}, \psi_{2k}, \psi_b, \lambda_k),$$
$$S = F(\psi, a_{1S}, a_{2S}, a_{3S}, \psi_{1S}, \psi_{2S}, \psi_b, \lambda_S), \tag{14}$$

Table 1
Parameters to simulate the experiment of Smith and Woolhiser (1971)

Parameter	Layer 1	Layer 2	Layer 3
Thickness (mm)	76.5	229.5	761
Ks (cm day^{-1})	566.9	365.7	268.2
θ_s	0.460	0.504	0.543
θ_r	0.020	0.025	0.025
ψ_b (cm)	−10.0	−13.0	−17.0
a_{1S}	0.8434	0.9163	0.9842
a_{2S}	−0.148	0.0143	0.170
a_{3S}	−0.260	−0.2028	−0.1549
ψ_{1S} (cm)	−12.85	−17.20	−25.18
ψ_{2S} (cm)	−2.80	−2.0	−2.0
λ_S	2.03	2.20	2.31
a_{1k}	0.5228	0.6229	0.7387
a_{2k}	0.204	0.1742	0.1071
a_{3k}	−0.09	−0.2197	−0.3179
ψ_{1k} (cm)	−13.73	−16.78	−21.34
ψ_{2k} (cm)	−1.0	−1.0	−1.0
λ_k	8.09	8.60	8.93

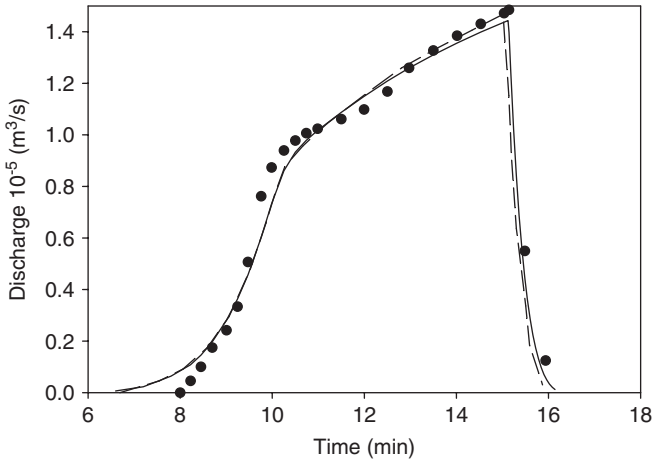

Fig. 1. Measured (symbols, Smith and Woolhiser (1971) and simulated (lines) hydrograph for the 12.2 m long and 1.22 m deep soil flume. ———— model of this work, - - - - model of Singh and Bhallamudi (1998).

where k is the unsaturated hydraulic conductivity, ψ is soil water potential, and F is a piece-wise function defined as

$$F(\psi, a_1, a_2, a_3, \psi_1, \psi_2, \psi_b, \lambda) = \begin{cases} (\psi_b/\psi)^{\lambda}, & \psi \leqslant \psi_1, \\ a_1 + a_2(\psi/\psi_b) + a_3(\psi/\psi_b)^2, & \psi_1 \leqslant \psi \leqslant \psi_2, \\ a_1 + a_2(\psi_2/\psi_b) + a_3(\psi_2/\psi_b)^2, & \psi > \psi_2, \end{cases} \quad (15)$$

subscripted a, ψ, and λ are parameters. Values of the parameters for the three sand layers are given in Table 1. The vertical spatial discretization steps varied from 0.001 m at the top to 0.05 m at the bottom, and the horizontal step was 0.25 m. Results of the hydrograph simulations are shown in Fig. 1. The model of this work performed with the same accuracy as the model of Singh and Bhallamudi (1998).

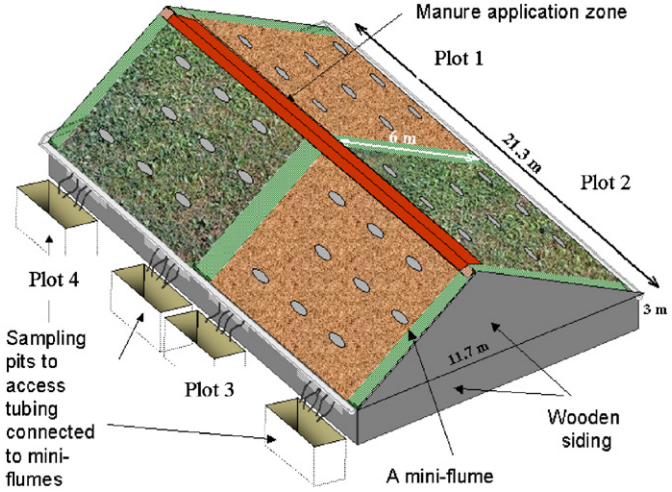

Fig. 2. Experimental setup to measure runoff transport of bromide and fecal coliforms released from manure under simulated rainfall.

2.2. Experimental data

The experimental site was located at Patuxent Wildlife Research Refuge (US Fish and Wildlife Services). A two-sided lysimeter (11.7 m × 21.3 m long) with 20° slope on both sides was instrumented to monitor the surface flow and transport, and infiltration rates (Fig. 2). Soil below the slope base level was confined with impermeable walls going down 3 m from the surface boundaries and impermeable bottom. Sandy loam soil was on one side of the lysimeter, and a 30-cm layer of clay loam soil overlays sandy loam on another side. Both sides had a gravel layer below 60 cm. Each side was divided into two plots, one bare, and another vegetated with the orchard grass. Each plot had a gutter at its base to collect runoff. A V-notch weir was installed at the end of the gutter to measure runoff rates. Triplets of mini-flumes were installed along three selected transects within each plot. The transects were located at 95, 285, and 490 cm from the top of the slope, and the gutter at the slope base was at 630 cm from the top. Mini-flumes were connected to the sampling pits outside the lysimeter with tubing buried about 20 cm below the soil surface. A four-nozzle rainfall simulator provided rainfall with the intensity of 6.1 cm h^{-1} and homogeneity coefficient 90% at the top four meters of the plot. Between 4 and 6 m from the top, the rain intensity linearly decreased to the zero value at the bottom of the plot.

Runoff plots were 6 m long. Soil was sampled for texture at the depths of 0–10, 10–30, 30–50, and 50–60 cm, and for water retention at 5–10, 20–25, 30–35, 40–45, and 55–60 cm depth intervals outside of the runoff plot area in triplicate. Soil texture was measured with the pipette method (Gee and Bauder, 1986), water retention was measured at the sand table and at the pressure plate at tensions of 0.1, 6, 13, 25, 50, 100, 330, 660 cm and of 1000, 5000, and 15,000 cm, respectively. Eq. (5) was fitted to the water retention data. Selected soil physical properties are given in Table 2.

Table 2
Soil texture and bulk density at the experimental plots

Depth (cm)	Soil texture									Bulk density		
	Plot 1 clay loam, bare			Plot 2 clay loam, grass			Plot 3 sandy loam, bare			Plot 1	Plot 2	Plot 3
	Clay	Silt	Sand	Clay	Silt	Sand	Clay	Silt	Sand			
0–10	39.2	31.0	29.9	38.7	40.2	21.2	13.0	26.5	60.5	1.40	1.48	1.66
10–30	34.2	32.5	33.3	35.5	36.3	28.2	14.3	17.7	68.0	1.41	1.50	1.69
30–55	22.7	18.2	59.1	20.6	16.2	63.2	13.7	16.3	70.0	1.52	1.56	1.67
55–60	24.9	11.7	63.4	16.6	14.9	68.5	13.9	17.2	68.9	1.61	1.61	1.65

Fresh manure was collected at the dairy farm the same morning it was applied. Twenty Kilograms of bovine manure was uniformly applied to the 30 cm wide strip at the top of each plot. The FC concentrations in manure were $(0.375 \pm 0.01) \times 10^6$, $(0.55 \pm 0.015) \times 10^6$, and $(2.8 \pm 0.12) \times 10^6$ as colony forming units (CFUs) per gram of manure in experiments at bare clay loam, vegetated clay loam, bare sandy loam, respectively; the "$\pm$" here and below separates the average and the standard deviation.

The potassium bromide solution was mixed with manure prior to application to provide a Br^- concentration of 2000 ppm. Rainfall was simulated for 1 h at bare plots, and for 1.5 h at the vegetated clay loam plot. At the vegetated sandy loam plot (Plot 4), 2 h of rainfall simulation did not provide a perceptible amount of runoff.

Runoff was collected during rainfall simulation for each consecutive 5-min interval in the gutter and from mini-flumes, and sampled to measure concentrations of FC and Br. After runoff simulations, water samples from mini-flumes were thoroughly mixed, and 50-ml subsamples were immediately taken to the laboratory for FC analysis. For FC analyses, unfiltered 50-μL runoff subsamples were plated on MacConkey Agar using an Autoplate 4000 spiral plater. The FC were counted using a Protocol plate reader (Synoptics, Cambridge, UK). Bromide concentration was measured with an ion-selective electrode (Orion, Thermo Electron Corporation, Woburn, MA, USA). An overview of the dataset and FC and Br mass balance computations are provided by Roodsari et al. (2005).

The setup of the experiment required model modification to account for discharge of runoff water and solutes to the mini-flumes. The infiltration rate computed from the solution of subsurface water flow equations was modified in the nodes corresponding to the mini-flume transects by adding the total volumetric mini-flume flux per area pertaining to such nodes as

$$I = I_{\text{inf}} + \kappa_{\text{m}} q \delta(l_i), \tag{16}$$

where I is the total infiltration rate present in Eq. (1), I_{inf} the infiltration rate from the solution of the subsurface flow equation, m s^{-1}; κ_{m} the hydraulic conductance of the mini-flumes, m^{-1}; q the runoff discharge per unit width, m^2/s; $\delta(l_i)$ the Dirac delta function, l_i the distance to the ith row of mini-flumes from the top of the slope, $i = 1,2,3$.

2.3. Model calibration

The Groundwater Modeling System (GMS) graphic user interface was used to prepare FEMWATER input files and to display simulation results. The IMSL Marquardt–Levenberg algorithm from the Digital Visual FORTRAN software package (Etzel and Dickinson, 1999) was used to fit the model to experimental data by adjusting flow and transport parameters for surface and subsurface. The model calibration was done separately for each plot. First, hydraulic properties were calibrated, and then the solute transport parameters were calibrated with previously found soil hydraulic properties. Calibrated hydraulic properties included (a) van Genuchten parameters α, n, θ_{r}, (b) the saturated hydraulic conductivity of topsoil and subsoil at the clay loam plots, and a single soil hydraulic conductivity value for the sandy loam plot, (c) the Manning roughness coefficient, and (d) the mini-flume hydraulic conductance, κ_{m}. Porosity was computed from bulk density. Calibrated solute transport parameters included (a) the manure release rate, K_{r}, h^{-1}, (b) the exponent p in the Eq. (8), (c) the dispersivity in the surface flow, m, and (d) the longitudinal dispersivity in soil, the partitioning coefficient in soil, K_{d}, and the surface straining rate, λ. Subsurface straining was not included in the simulations.

The transport models were calibrated with runoff flux data collected from the mini-flumes and gutter. The root-mean square values of residuals were minimized with the Marquardt algorithm. Residuals were computed as the differences between measured and simulated runoff fluxes, and as the differences between logarithms of measured and simulated Br and bacteria concentrations, to calibrate the flow and the transport model, respectively. Small parameter values $h_0 = 10^{-5}$ m, and $\omega = 0.001$ m were used in all computations. The spatial step along slope Δx was 0.1 m, and the vertical spatial increment varied from 0.001 m near the soil surface to 0.05 m at the bottom of the soil profile according to the power law $\mathrm{d}z_n = \mathrm{d}z_0 1.1^n$. A graphic user interface was developed for the run-time display of the model fitting process (not shown).

The objective function in the parameter estimation was the lack-of fit sum of squares:

$$\mathrm{LOFSS} = \sum_{j=1}^{M} n_j \left(\hat{Y}_j - \bar{Y}_j\right)^2, \tag{17}$$

where M is the total number of observations, n_j is the number of replicated measurements in the observation j, $\hat{Y}_j$ is the estimated-dependent variable for the observation j, $\bar{Y}_j$ is the average observed value of the dependent variable for the observation j. Values of fluxes and logarithms of concentrations were used as dependent variables in fitting flow and transport parameters, respectively.

The advantage of using Eq. (17) was the possibility for a direct comparison of model error and measurement error. The mean square lack-of-fit

$$s_\mathrm{r} = \sqrt{\frac{\mathrm{LOFSS}}{M-P}}, \tag{18}$$

is known to be an unbiased estimator of the model's error (Whitmore, 1991), P is the number of parameters of the model. The variability in measurements was evaluated with the standard deviation of measurements s_e obtained from data on replications:

$$s_\mathrm{e} = \sqrt{\frac{\sum_{j=1}^{M}\sum_{i=1}^{n}(Y_{ij} - \bar{Y}_j)^2}{\sum_{j=1}^{M} n_j - M}}, \tag{19}$$

where Y_{ij} is the ith replication of the measurement in the observation j. The model errors are significantly larger than intrinsic errors of measurements, if

$$\frac{s_r^2}{s_e^2} > F_{M-P,\sum_{i=1}^{M} n_j - M}, \tag{20}$$

where F is Fisher's ratio. The significance level of 0.05 was used. The determination coefficient R^2 of the linear regression 'simulated vs. measured values', was also computed to quantify the quality of the fits.

3. Results

3.1. Spatial and temporal variation in flow rates and solute concentrations

The mini-flume data demonstrated high variability between mini-flume triplets in rows. The variation coefficients in flow rates ranged from 20% to 120% and the average value was 65%. No temporal trend in variability was observed for the mini-flume flows. The middle mini-flume row had the lowest variability at clay loam plots and the highest variability at the sandy loam plot. The variation coefficients of the concentrations were also high across the rows of the mini-flumes (Fig. 3). For each row of mini-flumes, the variability in FC concentrations was higher than in Br concentrations at the clay loam plots, and the variation coefficients of FC and Br did not have a temporal trend (Fig. 3a and b). On the contrary, there was a similarity in the within-row variability of FC and Br concentrations at the sandy loam plot, and the variability decreased with time (Fig. 3c).

3.2. Flow data and simulations

Experimental hydrographs are shown in Fig. 4. Runoff was observed within 5 min on the bare clay loam plot and within 10 min on the bare sandy loam plot, but was not observed on the vegetated plot until after 40 min. Both vegetation and soil texture affected water balance. The cumulative runoff amounted to 93%, 60%, and 11% of the rainfall on the bare clay loam, bare sandy loam, and vegetated loam plots, respectively. The cumulative runoff was almost the same in all three mini-flume rows on the bare sandy loam plot, and increased from the first to third mini-flume row on the bare clay loam plot. On the

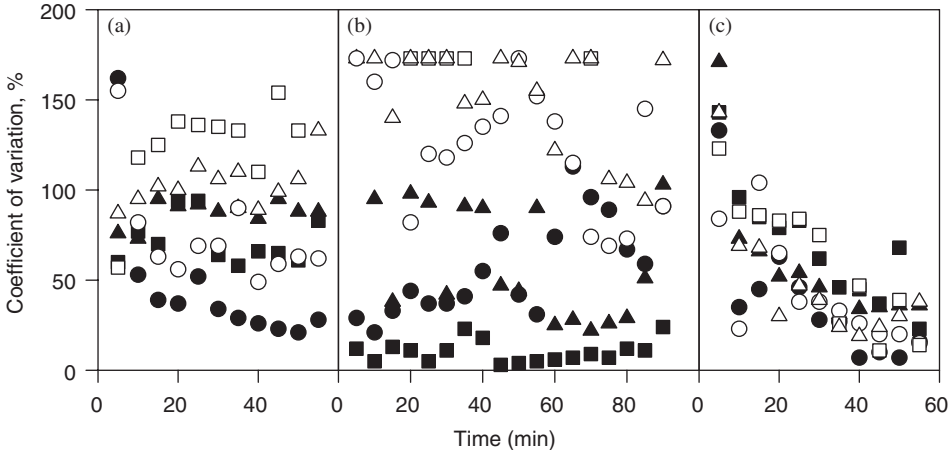

Fig. 3. Coefficients of variation of bromide (filled symbols) and fecal coliform (hollow symbols) concentrations in mini-flume outflow. ○, ●—95, □, ■—285 cm, △, ▲—495 cm from the top of the slope; *a*—bare clay loam, *b*—vegetated clay loam, *c*—bare sandy loam.

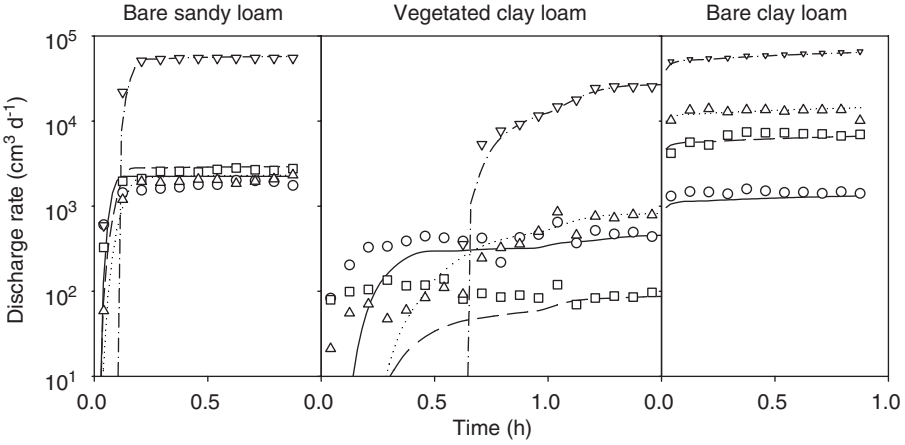

Fig. 4. Measured (symbols) and simulated (lines) runoff hydrographs; miniflumes—○, and ___—95 cm, □ and _ _ _—285 cm, △ and ••••—495 cm, ▽ and —•—•— —gutter.

Table 3
Estimated parameters of the surface and subsurface water flow and model performance statistics at three plots

	Plot 1-bare CL	Plot 2-grass CL	Plot 3 bare SL
Flow parameters			
Van Genuchten parameter α (m^{-1})	7.8	15.8[a]	12.3
Van Genuchten Parameter n	1.59	1.26[a]	1.75
Saturated water content θ_s (m^3/m^3)	0.38	0.34	0.36
Residual water content θ_r (m^3/m^3)	0.13	0.2	0.21
Manning roughness coefficient, m ($s\,m^{0.33}$)	0.04	20.00	6.98
Saturated hydraulic conductivity (topsoil), ($m\,h^{-1}$)	0.002	0.060	0.017
Saturated hydraulic conductivity (subsoil), ($m\,h^{-1}$)	NA	0.042	NA
Mini-flume conductance at 1st funnel line, κ_1 (m^{-1})	0.090	0.060	0.140
Mini-flume conductance at 2nd funnel line, κ_2 (m^{-1})	0.170	0.005	0.080
Mini-flume conductance at 3rd funnel line, κ_3 (m^{-1})	0.260	0.270	0.040
Model performance statistics			
s_r/AOR	0.059	0.068	0.021
R^2	0.95	0.98	0.87

[a]Subsoil parameters; s_r—the mean square lack-of-fit of the surface water flux simulations, $cm\,day^{-1}$, AOR—average total overland flux, $cm\,day^{-1}$.

vegetated clay loam plot, the first and the third mini-flume rows had the same cumulative runoff whereas the second row had much less runoff.

Table 3 shows calibrated parameters of the flow model and the model performance statistics. Plots in Fig. 4 and high determination coefficients, R^2, in Table 3 indicate that the flow model performed well. Calibrated saturated soil hydraulic conductivity values reflect differences in soil texture and flow conditions. The lowest

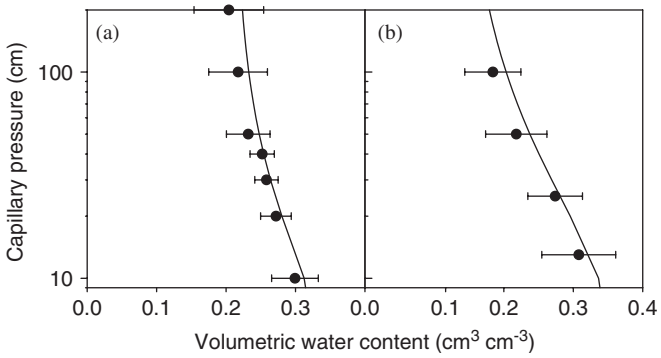

Fig. 5. Measured in topsoil (symbols) and estimated (lines) soil water retention; a—clay loam, b—sandy loam; the error bars show the 95% tolerance interval for measured water retention.

K_{sat} value was for the bare clay loam slope; vegetation substantially increased the saturated hydraulic conductivity (Table 3). Similar K_{sat} values were obtained for the sandy loam profile on the vegetated clay loam plot and for sandy loam subsoil at the vegetated clay loam. The smallest value of the roughness coefficient was found for the bare clay loam slope, whereas the largest value was for the vegetated clay loam. Differences in values of the mini-flume hydraulic conductances κ_m reflected the differences of mini-flume flow interception with respect to the mini-flume positions along the slope (Fig. 4 and Table 3). Calibrated and measured water retention compared favorably (Fig. 5).

3.3. Solute transport data and simulations

Bromide flux-averaged concentration data and simulation results are shown in Fig. 6. The top mini-flume row had the largest concentrations for all three plots. The gutter concentrations were the lowest for the bare clay loam plot. However, for two other plots, the gutter concentrations were higher than in the third mini-flume row. The Br mass

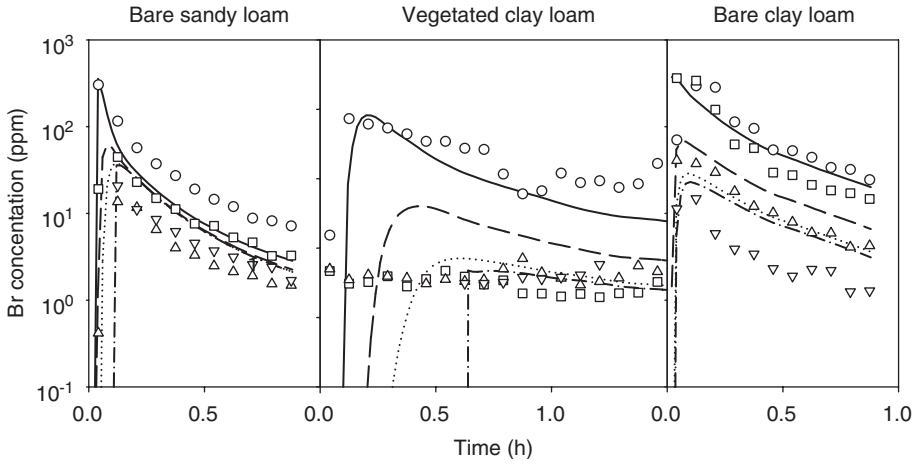

Fig. 6. Measured (symbols) and simulated (lines) bromide concentrations; mini-flumes—○, and ___—95 cm, □ and _ _ _—285 cm, △ and ••••—495 cm, ▽ and —•—•—gutter.

Table 4
Estimated parameters and performance statistics of the surface and subsurface bromide transport model at three plots

Transport parameter	Bare clay loam	Vegetated clay loam	Bare sandy loam
Manure release rate (h^{-1})	83.9	54.4	4.8
Exponent in the dependence of release rate on manure mass left	11.6	3.0	2.3
Dispersivity in the surface flow (m)	8.9	3.0	0.001
Topsoil dispersivity ($\times 10^3$, m)	5.6	10.8	8.5
Subsoil dispersivity ($\times 10^3$, m)	NA	35.2	NA
Surface straining rate (h^{-1})	0	10.1	0
Model performance statistics			
Mean square lack-of-fit, log(concentration)	0.26	0.42	0.28
Standard deviation of measurements in miniflumes log (concentration)	0.47	0.32	0.39
F-ratio	0.31	1.72	0.52
R^2	0.68	0.64	0.82

recovered in runoff was 97%, 32%, and 2% for the bare clay loam, bare sandy loam, and vegetated loam plots, respectively.

Parameters of the Br transport model and the model performance statistics are shown in Table 4. The surface straining rate approached zero as parameter estimation progressed for both bare plots, and converged to a non-zero value for the grass plots. In general, the model performed satisfactorily; the *F* ratios s_r^2/s_e^2 were all less than 2.0, which was the critical value at the significance level of 0.05; the lack-of-fit was not significant at this level. Nevertheless, the model could not explain the relatively high concentrations of Br in the first mini-flume of the bare sandy loam plot and relatively low Br concentrations in the gutter of the bare clay loam plot. Model errors in terms of logarithms of concentrations were largest for the vegetated clay loam plot 2. The largest absolute errors were encountered for the bare sandy loam (data not shown).

Fecal coliform flux-averaged concentration data and simulation results are shown in Fig. 7. A substantial similarity between FC and Br data (Fig. 6) was observed. The FC concentrations in the second and third mini-flumes on the bare sandy loam plot were comparable to the concentration in the gutter, which was not the case for Br concentrations. Also, the differences between concentrations of FC in mini-flumes and gutter were less than those of Br. The FC mass recovered in runoff was 68%, 23%, and 1% of that applied in manure on the bare clay loam, bare sandy loam, and vegetated clay loam plots, respectively.

Parameters of the model and the model performance statistics are shown in Table 5. Similar to Br transport, the surface straining rate converged to a non-zero value only on the vegetated plot. Both the variability in mini-flume measurements and the mean square lack-of-fit were larger for FC than for Br. In terms of *F*-ratios, the model performed satisfactorily, as the ratios s_r^2/s_e^2 were all less than the critical value of 2.0 at bare plots and slightly higher than critical at the vegetated plot.

Inspection of Br and FC transport parameters in Tables 4 and 5 showed that Br and FC parameters for the same plot were relatively comparable with respect to differences among plots. Therefore, an attempt was made to simulate FC transport using parameters found for Br. The model performance statistics for this case are given in Table 5. For bare plots, there was only a slight increase in the mean square lack-of-fit values, with some decrease in R^2 values. For the vegetated plots there was actually an improvement in the performance of the model; the mean square lack-of-fit value decreased and the R^2 value increased.

4. Discussion

Contamination of surface waters by manure-borne pathogens can occur as a result of both surface and

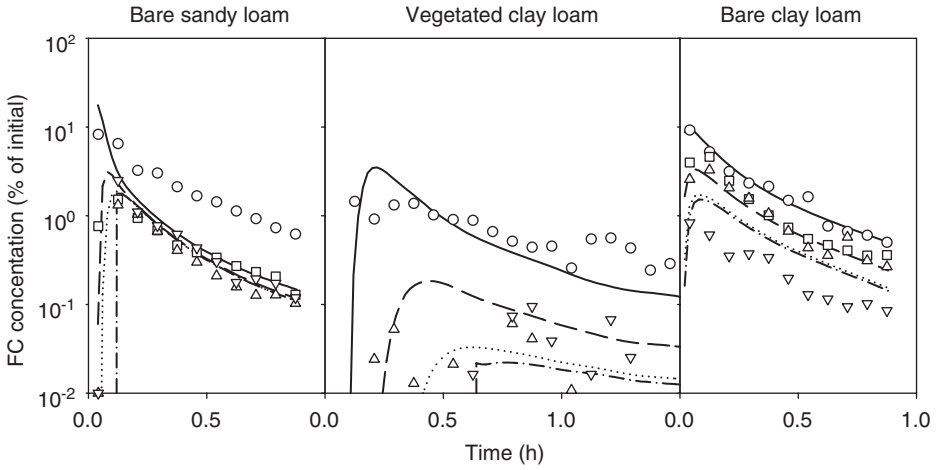

Fig. 7. Measured (symbols) and simulated (lines) fecal coliform concentrations; mini-flumes—○, and ___—95 cm, □ and _ _ _—285 cm, △ and ••••—495 cm, ▽ and —•—•—gutter.

Table 5
Estimated parameters and performance statistics of the surface and subsurface fecal coliform transport model at three plots

Parameter	Bare clay loam	Vegetated clay loam	Bare sandy loam
Manure release rate (h^{-1})	72	54	7.9
Exponent in the dependence of release rate on residual manure mass	6.1	3.0	2.4
Dispersivity in the surface flow (m)	12.0	3.0	0.07
Topsoil dispersivity ($\times 10^3$, m)	5.4	10.8	1
Subsoil dispersivity ($\times 10^3$, m)	NA	35	NA
Surface straining rate (h^{-1})	0	10	0
Partitioning coefficient in soil, K_d ($cm^3 g^{-1}$)	0.111	0.100	0.121
Model performance statistics			
Mean square lack-of-fit, log (concentration)	0.61	1.15	0.45
Standard deviation of measurements in mini-flumes log (concentration)	0.82	0.75	0.42
F-ratio	0.55	2.35	1.15
R^2	0.69	0.27	0.81
Model performance statistics in simulation of the fecal coliform transport with bromide transport parameters			
Mean square lack-of-fit, log (concentration)	0.66	0.66	0.51
R^2	0.68	0.47	0.71

subsurface microbial transport. The coupled surface–subsurface flow and transport modeling is needed to understand and forecast the relative effect of various processes. This work presents an attempt to investigate the feasibility of such a coupling to simulate manure-borne FC transport at the field scale. The size of the plots in this work (Fig. 2) was comparable with the sizes of VFSs used to prevent the transport of agricultural chemicals from fields and pastures to streams (Sanderson et al., 2001). One important feature of flow and transport at this scale is potential discontinuity of the surface flow due to the differences in soil infiltration capacity and micro-topographic differences (Fiedler et al., 2002). The boundary conditions of the subsurface flow in a unified form (11)–(13) eliminated the iterative steps required to find the ponding time in each of the surface nodes. This increased the computational efficiency of the code allowing for an accuracy of simulations that was comparable with previous algorithms developed to couple surface and subsurface flow (Fig. 1).

The three-dimensional flow domain was abstracted to two dimensions in this study. Experimental data in Fig. 3 show that substantial variability in flow and transport can occur within the VFS. Simulations of Br and FC concentrations were least successful for the mini-flumes closest to the source, at 65 cm from the application area (Figs. 6 and 7). This could be related to the channeled surface flow of the manure from the application area along the bare slopes (Raff et al., 2003), and to the transport of Br and FC with relatively large manure particulates that became strained on the grass slope (Ghadiri et al., 2002). Surface-channeled transport pathways have previously been documented in runoff studies on vegetated slopes, (i.e., Stutter et al., 2005). At larger distances, the two-dimensional representation of the flow and transport became satisfactory, and the advective–dispersive model was able to capture the variations in transport across the slope within the advective–dispersive flow hypothesis. As defined by concentrations that were flux-averaged across mini-flumes, the breakthroughs for bare plots were relatively sharp (Figs. 6 and 7). The surface dispersivity was the largest for the bare clay loam plot where the surface channeling was visible during the experiments (Tables 4 and 5). Intermediate values of dispersivity were found for the vegetated plots where the presence of grass litter and residue could create some flow channeling. The smallest value was encountered for the sandy loam bare plot. Such small values justified the adaptation of the front limitation algorithm of Haefner et al. (1997) to the surface transport problems in this study.

Because the soil in the vegetated clay loam plot had a sandy loam texture below 30 cm, both topsoil and subsoil K_{sat} had to be calibrated (Table 3). In the bare clay loam plot, the soil also had the sandy loam subsoil; however, the total infiltration was relatively small, only about 5 mm, and subsoil properties did not affect the simulation results.

Water retention of the clay soil decreased substantially at very low capillary pressures (Table 3 and Fig. 5), and this is reflected in parameters in Table 3 (large n and α values). The shape of the water retention curves indicates the presence of connected large pores that are being emptied at low capillary suctions as the capillary suction increases. Interaggregate pore space or cracks probably represent such pores.

We realize that the estimates of both water retention parameters and hydraulic conductivity at bare plots could be affected by surface sealing or crusting. Data on soil water profile distribution are needed to calibrate submodels of sealing or crusting. We obtained such data with the capacitance probes (not shown), but they were highly spatially variable. We were not aware of an experimental method that would allow us to independently evaluate the effect of hillsope sealing or crusting on runoff and infiltration. Therefore we did not include sealing and/or crusting in the model.

The decrease of Br and FC concentration along the slope and with time reflected both dilution in the overland flow and the kinetics of the Br and FC release from manure. We first applied a simple exponential-with-time release model, i.e. Eq. (8) with the exponent $p = 0$. The shape of the concentration time series was dissimilar to the observed data (data not shown). The surface transport simulations improved when the exponent p was allowed to vary, which corresponded to a relative slowdown in release as time progressed. A possible explanation is that the fast release of liquid manure components was followed by a slower dissolution of solid components. A similar slowdown has been observed in other studies in which different release models were proposed (Bradford and Schijven, 2002; Vadas et al., 2004). Parameters of the manure dissolution model were different for different plots in those works, probably because manure consistency was variable. These experiments were conducted at 14-day intervals.

Surface straining had to be accounted for to simulate surface transport on the vegetated slopes but not on the bare slopes. This may mean that both Br and bacteria are co-transported with manure particulates and can be retained by vegetation, litter, and micro-ponds. This corresponds to the conclusions of Ghadiri et al. (2002) that the VFS behaves like porous barriers against the flow, creating zones with increased flow depth or backwater whose length varies with slope angle and vegetation density.

The same release and transport parameters could be used in simulations of both Br and FC in this work. This may concur with the conjecture of Edwards et al. (1996a, b) that manure-borne constituents are transported primarily in the solution phase. However, this may also mean that manure particulates carry bacteria and move in the runoff suspension without substantial gravitational deposition, because their bulk density is only slightly greater than that of water. Similarities in transport of manure particulates and Br in stony soil were observed (Shelton et al., 2003). It remains to be seen whether manure particulates carry a substantial amount of bacteria or they just move with water, and that bacteria are mostly in the liquid phase.

5. Conclusions

Combining the Saint-Venant model for overland flow, the Richards equation for variably saturated flow in soil, and the advective–dispersive transport equations for surface and subsurface transport provided a satisfactory representation of manure-borne Br and FC transport on slopes under simulated rainfall at field scale. Transport parameters for surface runoff appeared to be comparable for manure-borne FC and bromide-ion. The flexible model developed for this study is suitable for simulating surface and subsurface transport of agricultural contaminants on hillslopes. It shows promise for evaluating the efficacy of the vegetated filter strips.

References

Abu-Zreig, M., Rudra, R.P., Whiteley, H.R., Lalonde, M.N., Kaushik, N.K., 2003. Phosphorus removal in vegetated filter strips. Journal of Environment Quality 32, 613–619.

Bartfield, B.J., Blevins, R.L., Fogle, A.W., Madison, C.E., Inamdar, S., Carey, D.I., Evangelou, V.P., 1998. Water quality impact on natural filter strips in karst areas. Transactions of the ASAE 41, 371–381.

Bradford, S.A., Schijven, J., 2002. Release of *Cryptosporidium* and *Giardia* from dairy calf manure: impact of solution salinity. Environmental Science and Technology 36, 3916–3929.

Crane, S.R., Moore, J.A., Gismer, M.E., Miller, J.R., 1983. Bacterial pollution from agricultural sources. A review. Transactions of the ASAE 26, 858–872.

Edwards, D.R., Daniel, T.C., Moore Jr., P.A., 1996a. Vegetative filter strip design for grassed areas treated with animal manures. Applied Engineering in Agriculture 12, 31–38.

Edwards, D.R., Moore Jr., P.A., Daniel, T.C., Srivastava, P., 1996b. Poultry litter- treated length effects on quality of runoff from fescue plots. Transactions of the ASAE 39, 105–110.

Etzel, M., Dickinson, K., 1999. Digital Visual Fortran Programmer's Guide. Digital Press, Elsevier, New York, Amsterdam.

Fiedler, F.R., Frasier, G.W., Jorge, A., Ramirez, J.A., Ahuja, L.R., 2002. Hydrologic response of grasslands: effects of grazing, interactive infiltration, and scale. Journal of Hydrologic Engineering 7, 293–301.

Gee, G.W., Bauder, J.W., 1986. Particle-size analysis. In: Klute, A. (Ed.), Methods of Soil Analysis. Part 1. Physical and Mineralogical Methods. American Society of Agronomy, Madison, WI, pp. 399–404.

Ghadiri H., Rose, C.W., Misra, R.K., 2002. Buffer-strip induced flow retardation and sediment deposition. Proceedings of the 12th ISCO Conference Beijing 2002, pp. 163–168.

Haefner, F., Boy, S., Wagner, S., Behr, A., Piskarev, V., Palatnik, B., 1997. The front limitation algorithm: a new and fast finite-difference method for groundwater pollution problems. Journal of Contaminant Hydrology 27, 43–61.

Johnson, G.D., Moore, L.A., 1978. The Effect of Conservation Practices on Nutrient Loss. Department of Agriculture Engineering University of Minnesota, 227pp.

Kouznetsov, M.Y., 1989. Development and use of mathematical models of water transfer at irrigated lands. Ph.D. Thesis. Research Institute of Heat and Mass Transfer, Minsk, 170pp.

McCaskey, T.A., Rollons, G.H., Little, J.A., 1971. Water quality of runoff from grassland applied with liquid, semi-liquid, and 'dry' dairy waste. In: Livestock Waste Management and Pollution Abatement. Proc. 2nd Intern. Symp. on Livestock Wastes. ASAE. St. Joseph, MI, pp. 239–242.

Raff, D.A., Smith, J.L., Trlica, M.J., 2003. Statistical descriptions of channel networks and their shapes on non-vegetated hillslopes in Kemmerer, Wyoming. Hydrological Processes 17, 1887–1897.

Richards, D.R., Lin, H.J., Yeh, G., Cheng, H., Cheng, J., 1997. FEMWATER: a three-dimensional finite element computer model for simulating density-dependent flow and transport in variably saturated media. Report A769723. Army Engineer Waterways Experiment Station, Vicksburg MS.

Roodsari, R.M., Shelton, D.R., Shirmohammadi, A., Pachepsky, Y.A., Sadeghi, A.M., Starr, J., 2005. Fecal coliform transport as affected by surface condition. Transactions of ASAE 48, 1055–1061.

Sanders, B., Iahr, M., 2001. High resolution and non-oscillatory solution of the St. Venant equations in non-rectangular and non-prismatic channels. Journal of Hydraulic Research 31, 321–330.

Sanderson, M.A., Jones, R.M., McFarland, M.J., Stroup, J., Reed, R.L., Muir, J.P., 2001. Nutrient movement and removal in a switchgrass biomass-filter strip system treated with dairy manure. Journal of Environmental Quality 30, 210–216.

Shelton, D., Pachepsky, Y.A., Sadeghi, A.M., Stout, W.L., Karns, J.S., Gburek, W.J., 2003. Release rates of manure-borne coliform bacteria from data on leaching through stony soil. Vadoze Zone Journal 2, 34–39.

Singh, V., Bhallamudi, M., 1998. Conjuctive surface-subsurface modeling of overland flow. Advances in Water Resources 21, 567–579.

Smith, R.E., Woolhiser, D.A., 1971. Overland flow on an infiltrating surface. Water Resource Research 7, 899–913.

Stutter, M.I., Deeks, L.K., Billett, M.F., 2005. Transport of conservative and reactive tracers through a naturally structured upland podzol field lysimeter. Journal of Hydrology 300, 1–19.

Vadas, P.A., Kleinman, P.J.A., Sharpley, A.N., 2004. A simple method to predict dissolved phosphorus in runoff from surface-applied manures. Journal of Environmental Quality 33, 749–756.

Van Genuhten, M.T., 1980. A closed-form equation for predicting the hydraulic conductivity of unsaturated soils. Soil Science Society of America Journal 44, 892–898.

Whitmore, A.P., 1991. A method for assessing the goodness of computer simulation of soil processes. Journal of Soil Science 42, 289–299.